Finite conjugate embedded relay lens hyperspectral imaging system (ERL-HIS)

Yao-Fang Hsieh,[1] Mang Ou-Yang,[2,*] and Cheng-Chung Lee[1]

[1]Department of Optics and Photonics, National Central University, 300 Jhongda Road, Chungli City, Taoyuan County 32001, Taiwan

[2]Department of Electrical Engineering, National Chiao-Tung University, 1001 University Road, Hsinchu City 30010, Taiwan

*Corresponding author: oym@cc.nctu.edu.tw

Received 17 August 2011; revised 16 October 2011; accepted 21 October 2011; posted 24 October 2011 (Doc. ID 153052); published 15 November 2011

We present a novel embedded relay lens hyperspectral imaging system (ERL-HIS) with high spectral resolution (nominal spectral resolution of 2.8 nm) and spatial resolution ($30\,\mu m \times 8\,\mu m$) that transfers the scanning plane to an additional imaging plane through the internal relay lens so as to alleviate all outside moving parts for the scanning mechanism used in the traditional HIS, where image scanning is achieved by the relative movement between the object and hyperspectrometer. The ERL-HIS also enables high-speed scanning and can attach to a variety of optical modules for versatile applications. Here, we also demonstrate an application of the proposed ERL-HIS attached to a microscopic system for observing autofluorescent images of sliced cancer tissue samples.

OCIS codes: 110.4234, 120.6200, 170.3880, 170.3890.

1. Introduction

According to Willoughby *et al.*, a hyperspectral image consists of tens or hundreds of spectral bands, at the spectral resolution in the order of 0.01 [1]. By adding the other two dimensions, namely the y axis, representing the slit direction of the optical system, and the x axis, representing the scanning direction, a hyperspectral image can be regarded as a collection of many two-dimensional (2D) images measured at different wavelengths to form a data cube ($x \times y \times \lambda$). The hyperspectral image has been widely applied to many areas, such as macroscopic image examination, documentation or artistic and historic object inspection, and biomedical fluorescence imaging [2,3]. Recent advances in biomedical optics have led to the widespread use of the hyperspectral image in microscopy [4–6].

Three major methods of measuring a hyperspectral image involve scanning in the wavelength, spatial, or time domains [7]. The proposed embedded relay lens hyperspectral imaging system (ERL-HIS) uses a scanning technology in the spatial domain, which is achieved by using a scanning relay lens (RL) module consisting of a RL and a stepping motor (SM). Unlike the traditional HIS [Fig. 1(a)] based on the scanning mechanism relying upon relative movements between the object and hyperspectrometer (HM), the proposed ERL-HIS [Fig. 1(b)] can only be achieved by moving either the object or the HM. The former may need a bulky and complex scanning mechanism, which in general costs more compared to the proposed ERL-HIS. As seen in Fig. 1(b), the RL is placed inside the optical module (OM). The thick dotted line denotes the optical path of the OM, while the thin dotted line represents the optical path of the RL. The RL is specially designed with symmetric infinite conjugate lenses for scanning objects and transferring images with minimal off-axis optical aberration (distortion $< 0.01\%$, field curvature$< 0.2\,\mu m$). Although the ERL-HIS adds the RL part, the entire volume is still smaller than the conventional system. Because the RL system can effectively

0003-6935/11/336198-08$15.00/0

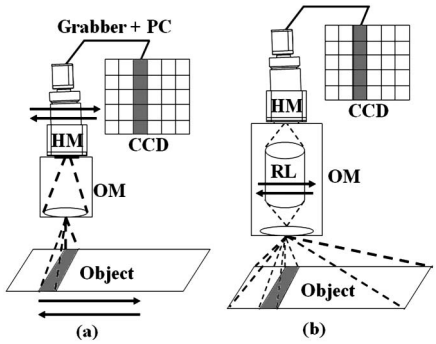

Fig. 1. Sketch of (a) a conventional system and (b) the proposed ERL-HIS.

span the spatial space with appropriate separation, the proposed system can optically change the moving mechanism of nanometer-level resolution needed in a traditional HIS, which can only be achieved by using a piezoelectric transducer (PZT), to that of micrometer-level resolution. The latter can be easily accomplished by an ordinary SM, which may dramatically lower the cost of an HIS.

The conventional HIS has been, in general, based on either a reflective or pushbroom scanning mechanism [8,9]. These scanning mechanisms had certain limitations. The reflective hyperspectral system utilized an autorotating reflective mirror as the scanning mechanism. With a different scanning angle, different optical paths may cause optical aberrations. Such a system had more off-axis aberration than the ERL-HIS and cannot be used for large-scale scan in a short distance. Also, the distortion was obvious at the edge of an image. The other conventional scanning mechanism was the pushbroom structure. The mechanism of pushbroom hyperspectral system was more complex and larger than the ERL-HIS. The off-axis aberration was more pronounced than that of an ERL-HIS. Furthermore, a sample object was normally required for scanning by using a long travel distance and highly accurate scanning platform driven by PZT, which was more expensive than the SM.

Recently, the snapshot hyperspectral images that can simultaneous acquire spatial and spectral information without scanning have been widely applied to biological microscopy, such as the coded aperture snapshot spectral imager (CASSI) [10], computed tomography imaging spectrometer (CTIS) [11], and snapshot image mapping spectrometer (IMS) [12,13]. The CASSI and CTIS can acquire data in real time, but they cannot show the full-resolution data cube in real time because the computation was complex and massive. The principle of IMS was upon recognizing areas (pixel and lines) of the sample's image on a large-format CCD for spectral spread and simultaneous data cube acquisition. The IMS can acquire a data cube of dimensions $285 \times 285 \times 60\,(x, y, \lambda)$ with spatial resolution (~0.45 mm) and spectral resolution (~8 nm) in the case of a 40× objective. The advantages of IMS were acquiring the data cube in real-time, not needing to scan object, and increasing a single channel's signal to noise ratio. However, the limitations were the narrow wavelength range (~60), lower imaging format (285 × 285), and low throughput (~20%).

To our best knowledge, this is the first time that a scanning RL module has been applied to a hyperspectral imaging system. The proposed ERL-HIS has several advantages over the pushbroom or reflective hyperspectral system: the proposed system is characterized by its higher scanning speed (1000 × 1000 pixels with 200 spectral bands about every 30 s); compact volume of the RL module; attachable to various OMs with simple alignment; controllable exposure time; and selectable region of interest (ROI), which means that the designated region and spectral bands of the object could be chosen and scanned to decrease the acquisition time. Furthermore, the proposed system can increase the spatial resolution of an image through magnifying the image using the front OM, and it has lower off-axis optical aberration compared to the conventional HIS. In this paper, the design and development of ERL-HIS is reported. The acquired data cube is of size $1000 \times 1000 \times 200\,(x, y, \lambda)$. We also demonstrate an application of the ERL-HIS attached to the microscope (Olympus U plane super apochromat objective 10×) for observing *in vitro* sliced cancer tissue samples. In this case, the spatial resolution is $3\,\mu\text{m} \times 0.8\,\mu\text{m}$ and the nominal spectral resolution is about 2.8 nm covering the wavelength range from 400 to 1000 nm.

2. Finite Conjugate Relay Lens

A. Design Principle

This section describes the design principle and important optical parameters of the RL. In the first part, the concept of the finite conjugate and infinite conjugate is introduced. A finite conjugate system implies that while a light source (not at infinity) passes a system, it focuses on a particular spot. An infinite conjugate system implies that while a collimated (parallel) light passes a system, it changes the beam diameter according to the magnification and emits the collimated light [14]. The RL resembles a finite conjugate optical system with unity transverse magnification. The RL we designed here utilizes the finite conjugate OM consisting of two symmetrically infinite conjugate lenses with the same focus point to cancel aberration. Because the system could form an extra image of real objects at a finite distance, the RL system can carry an image through a distance, but with a limited diameter of the lenses [15]. The RL system is also a telecentric system. The telecentric system implies that the exit pupil of an optical system is at infinity and the image size remains constant with the variation of focus. Because of the property of telecentricity, the off-axis image remains the same as the central image; in addition, even if the light focus changes, it does not affect the image size and thus minimizes image

distortion. The RL system consists of 14 lenses. The 5th and 6th lenses were designed to calibrate the lateral color aberration. There are 31 surfaces in the RL. The aperture stop is located on 16th surface. The size of the aperture stop is about 4.77 mm. The total length of the RL is about 124 mm, the magnification −1, the $F/\#2.8$, the effective focal length about 1000 mm, the back focal length about −1000 mm, the entrance pupil diameter about 750 mm, the exit pupil diameter about 750 mm, the entrance pupil position about 2000 mm, the exit pupil position about −2000 mm, and the image height about 7.25 mm.

B. Simulations of the Relay Lens

The ZEMAX program was used to simulate the optical system and evaluate its performance. This was followed by experiments to verify the performance of the actual system that we had constructed. Figure 2 schematically depicts a 2D layout of the RL. Figures 3–6 summarize the results using the initial design of the RL. The modulation transfer function (MTF) refers to the ability of an optical system to capture image contrast over a range of spatial frequency. Figure 3 plots the MTF result of the RL in three fields, where 0 mm denotes the central field of the RL and 7.25 mm is the marginal field. The MTF in a tangential plane was better than that in a sagittal plane in all fields except for the 7.25 mm field. The optical performance appeared to be stable in all fields. Figure 4 shows the spot size in all fields. The maximal root mean square (rms) radius was 13.05 μm in the 7.25 mm field. The minimal rms radius was 9.344 μm in the 4 mm field. Figure 5 indicates that the image distortion is lower than 0.01% and the field curvature is smaller than 0.2 μm. The RL projected the image onto the scanning plane and produce excellent imaging quality. Figure 6 shows a lateral color smaller than 0.4 μm from wavelengths 400 to 1000 nm. Notably, the lateral color shift affected the image quality the most when the RL was applied to a hyperspectral imaging system. The simulation results showed that the RL design was able to deliver high-quality images all over the entire optical field.

C. Experiment of the Relay Lens

This paragraph describes an experiment to further confirm the simulation results. Figure 7 shows the experimental setup for testing the optical performance of the RL. The optical components included the RL, a two-axis platform, charge-coupled device (CCD) sensor, and collimator. The MTF was measured by the standard slanted edge approach [16].

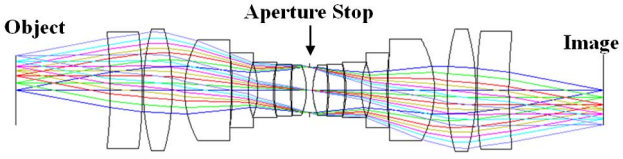

Fig. 2. (Color online) 2D layout of the RL.

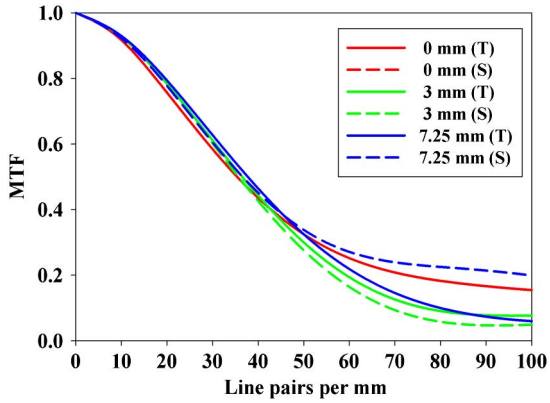

Fig. 3. (Color online) MTF of the RL.

The collimator was used as light source. The negative 1951 USAF resolution target was used as the test pattern, which was inserted into the collimator. On the CCD plane, the image of the pattern could be regarded as an edge spread function, which was differentiated to obtain the line-spread function (LSF). The MTF was derived from the transformed LSF using the Fourier transform. Figures 8 and 9 show the tangential and sagittal directions of the MTF. The simulation and experimental MTF results resembled each other. The sagittal MTF of the 7.25 mm field was also better than that of the 0 mm field. The cut-off frequency was about 89 lp/mm, because the CCD pixel size was 5.6 μm.

3. Embedded Relay Lens Hyperspectral Imaging System

A. Operational Principle of the ERL-HIS

This section describes the operating principles and components of the ERL-HIS. Figure 10 schematically depicts a conceptual drawing of the ERL-HIS. The

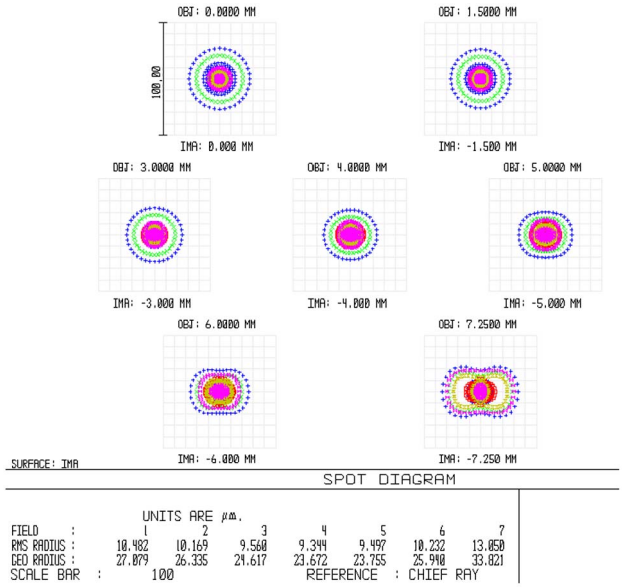

Fig. 4. (Color online) Spot size of the RL.

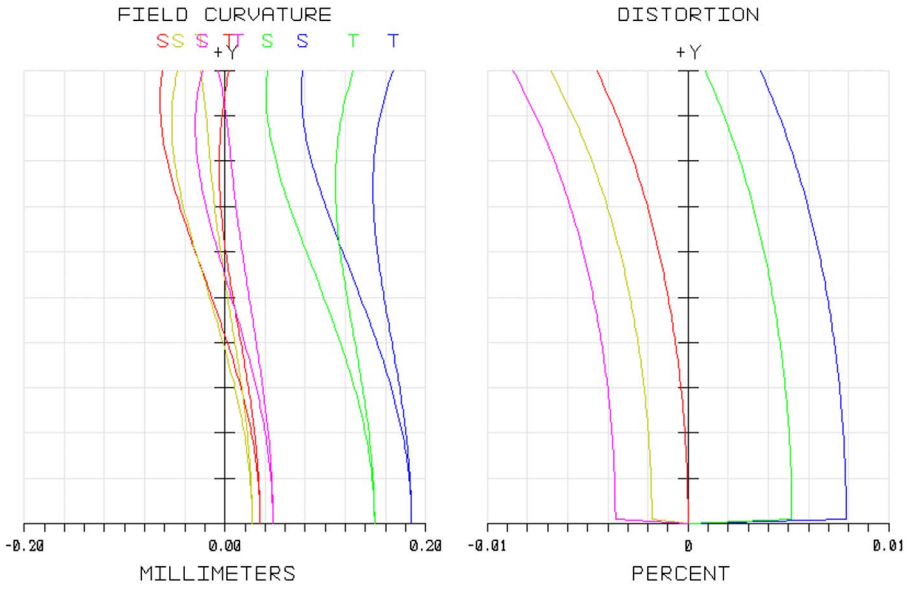

Fig. 5. (Color online) Field curvature and distortion of the RL.

OM collects radiation from the object and forms an image on image plane 1 (ImP1). The RL projects the image from Image plane 1 (ImP1) to image plane 2 (ImP2), which is the slit of the hyperspectrometer. The slit is located in the y axis and has a width of 30 μm and allows for ImP2 imaging one line at a time on the electron multiplying charge-coupled device (EMCCD). Despite the RL projects, the circle image from ImP1, the image of ImP2 is limited by the slit size. The collimating optics (CO) can collimate the image to the dispersive (D) structure, and the dispersive structure then disperses the image. The dispersive element of the hyperspectrometer is a prism–grating–prism structure. Finally, the image is focused on the EMCCD by the focusing optics (FO). Therefore, while the RL is static, the image of a slit size and its spectrum can be recorded on the EMCCD. As the SM scans along the x axis, the individual line image is recorded in the y–λ plane on the EMCCD. The SM moves one step in the x axis to acquire the next line image and its spectrum. Each y–λ image is recorded as a single y–λ file for each row along the object corresponding to the radiation collection region, which maps through the hyperspectrometer to the EMCCD. After all of the line images are acquired, the data cube of all of the y–λ files is loaded to memory. Figure 11 shows the finished product of the ERL-HIS, which consists of a mount, RL, SM (Sigma Koki, SGSP20-20), hyperspectrometer (Specim V10E), and EMCCD (Andor Luca R604). Because the mechanism of the ERL-HIS is straightforward, the optical alignment is easy to perform. The ERL-HIS can connect to various OMs through different mounts for different applications. The volume of the ERL-HIS is about 50 cm (L) × 15 cm (W) × 13 cm (H). The volume of the RL module that is composed of RL and SM is about 20 cm (L) × 15 cm (W) × 13 cm (H). When a different hyperspectrometer has been connected to the RL modules, the wavelength range (400 to 1000 nm in this study) can be easily extended. The EMCCD used in this study produced high-resolution images (1000 × 1000 pixels) with a small pixel size (8 μm × 8 μm), high dynamic range (14 bits), and high frame rate (12.4 frames per second). The software was written in C language to control the

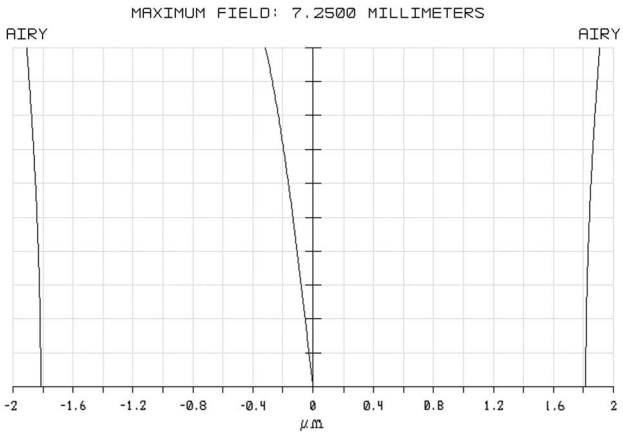

Fig. 6. Lateral color of the RL.

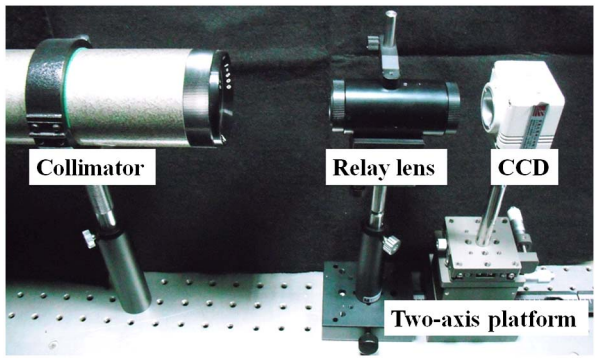

Fig. 7. (Color online) Setup of MTF measurement.

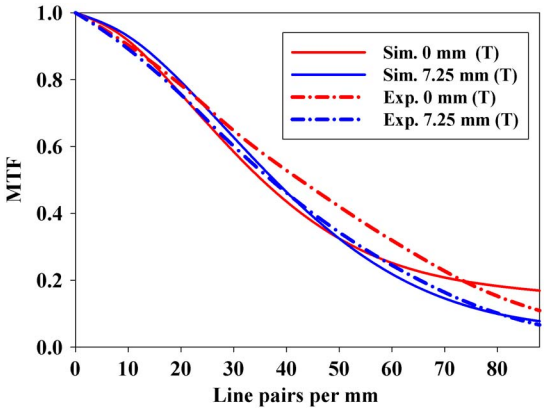

Fig. 8. (Color online) Tangential MTF of the RL.

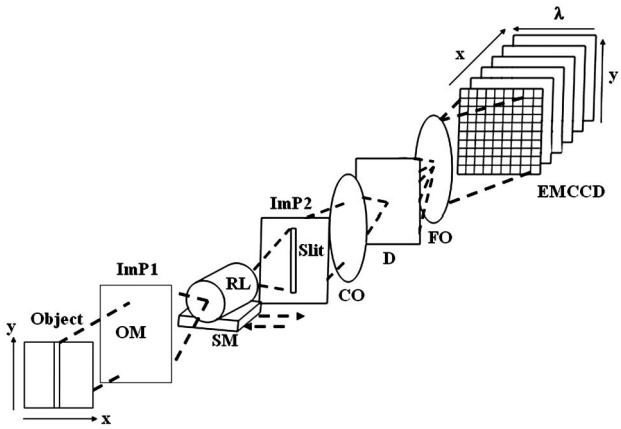

Fig. 10. Operation principle of the ERL-HIS.

hardware for imaging acquisition and to analyze and display the spectral information of the selected ROIs. The software was also capable of controlling the speed of the SM, exposure time, gain and the binning number of the EMCCD, and the spectral images to be combined for the resultant image displayed on the software window.

B. ERL-HIS Analysis

This section describes the analysis results of spatial resolution, spectral resolution, and image aspect ratio of the proposed system. The spatial resolution of the ERL-HIS can be discussed in the x axis and the y axis, respectively. The spatial resolution of the x axis is determined by the entrance slit width of the hyperspectrometer, number of pixels binned in the x axis of the EMCCD, and the magnification of the front OM. Because the magnification of the RL is −1, the RL does not affect the spatial resolution of the proposed system. The slit width of the proposed system is 30 μm, and the bin size of the x axis of the EMCCD is set to 1. Thus, the spatial resolution of the x axis of the proposed ERL-HIS is 30 μm. The spatial resolution of the y axis is determined by the pixel size of the EMCCD, the bin size of the y axis of the EMCCD, and the magnification of the front OM. The pixel size of the EMCCD is 8 μm, and the bin size of the y axis is set to 1. Hence, the spatial resolution of the y axis of the proposed ERL-HIS is 8 μm. However, when the system attaches to a microscope, the magnification of the objective lens affects the spatial resolution. For the 10× objective, the spatial resolution of the entire system is 3 μm × 0.8 μm.

The spectral resolution (generally referred as the nominal spectral resolution) of a hyperspectral imaging system means the width of an individual spectral channel. The nominal spectral resolution is defined by the slit width of the hyperspectrometer, and it is normally calculated by the slit width ratio. For the 80 μm slit width, the nominal spectral resolution is about 7.5 nm. Because the slit width of the ERL-HIS is 30 μm, the nominal spectral resolution is about 2.8 nm. The full width at half maximum is 2.79 nm when the peak of the measurement light is at 435.8 nm, 3.06 nm when the peak is at 696.5 nm, and 3.17 nm when the peak is at 912.3 nm.

The image aspect ratio is also an important parameter of the proposed ERL-HIS system, and it depends on the number of steps of the SM. The SM must move the appropriate number of steps for each scan line, which means each exposure time of EMCCD. Figure 12 shows the image aspect ratio in a different number of steps for each scan line. The number of steps for each scan line must be the same as the spatial resolution of the y axis. For the one pixel binned, the spatial resolution of the y axis is 8 μm. The SM has precision of 2 μm per step. Thus, the appropriate number of steps is four for each scan line. When the number of steps is three, the image aspect ratio is 0.67 [Fig. 12(a)]. When the number of steps is five,

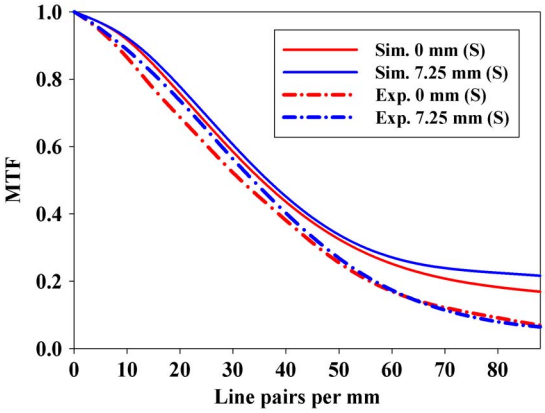

Fig. 9. (Color online) Sagittal MTF of the RL.

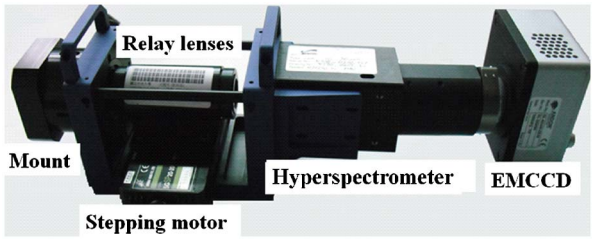

Fig. 11. (Color online) Finished product of the ERL-HIS.

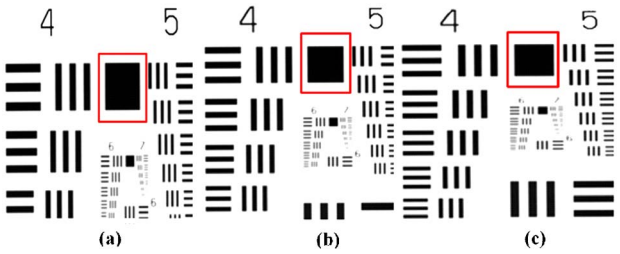

Fig. 12. (Color online) Image aspect ratio in different number of steps: (a) image aspect ratio of 0.67 with the number of steps being 3, (b) image aspect ratio of 1 with the number of steps as 4, and (c) image aspect ratio of 1.33 with the number of steps as 5.

the image aspect ratio is 1.33 [Fig. 12(c)]. Both create images with the wrong x–y aspect ratio.

C. Experiments and Results of ERL-HIS

This section describes the system calibration results and related experiments. Spectral and radiometric calibration were performed on the proposed system. The spectral calibration ensures each pixel represents the correct wavelength. An Hg-Ar lamp (SphereOptics) was used as the light source for calibration. The spectrum of the Hg-Ar lamp was measured by the spectrometer (SphereOptics SMS-500) and the proposed system. The characteristic wavelength of the Hg-Ar lamp should be in the same position of these two instruments. Figure 13 shows the calibration results of the proposed system. The characteristic wavelength of the proposed system was the same as that of the spectrometer after calibration.

Radiometric calibration was also important work for the ERL-HIS. The spectral response curve of the EMCCD required calibration, because the peak quantum efficiency of each wavelength was different. A halogen lamp was used as the standard light source for calibration. Initially, a dark image with no light to the EMCCD was used to remove the noise interference of the proposed system. Next, a reference blank was used to remove nonuniformity in the image caused by uneven illumination; periodic scan

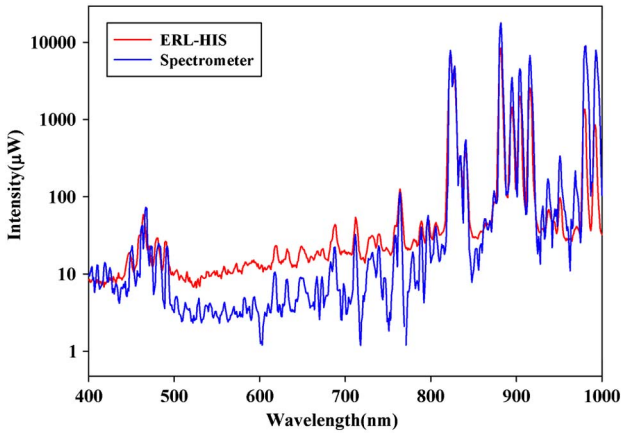

Fig. 13. (Color online) Result of spectral calibration from 400 to 1000 nm. The longitudinal coordinate has been taken as a logarithm.

line stripping; and the impact of the lamp, medium, and reflectance and transmittance of the sample. The spectral response curve of a standard light source was different with the ERL-HIS system from 400 to 1000 nm. The k value is defined as the calibrated parameter. According to Eq. (1), k is defined as the spectral response values of a standard light source that divides the spectral response values of the ERL-HIS, where $S(\lambda)$ denotes the response value of standard light source of each wavelength and $H(\lambda)$ represents the response value of the proposed system for each wavelength. Figure 14 shows the k value of each wavelength. Therefore, the intensity of each wavelength of the EMCCD must multiply the correspondent k value. According to the results, the calibration coefficient was less than 9 dB. The 9 dB were calculated from $10 \times \log(80/9)$. Notably, 80 is the maximum value of k, and 9 is the minimum value of k. The calibration was thus validated:

$$k = \frac{S(\lambda)}{H(\lambda)}. \tag{1}$$

Figure 15 shows the MTF of the ERL-HIS. The cut-off frequency was about 62 lp/mm, because the EMCCD pixel size was 8 μm. The tangential MTF was 30%, while the sagittal MTF was 20% at 62 lp/mm. The reliability of the proposed system was also demonstrated by attaching it to a microscope to acquire images of oral cells. Figure 16 shows the attachment of the ERL-HIS on the microscope. The setup added the CCD (AVT PIKE F-421C) on the right side. The sample under observation can be previewed by the right-side CCD before using ERL-HIS to acquire the image. Following the preview, the ERL-HIS can select the ROI to analyze the spectral information. The image on the monitor was superimposed by the wavelengths of 450, 550, and 650 nm. The software allowed users to select resultant images of

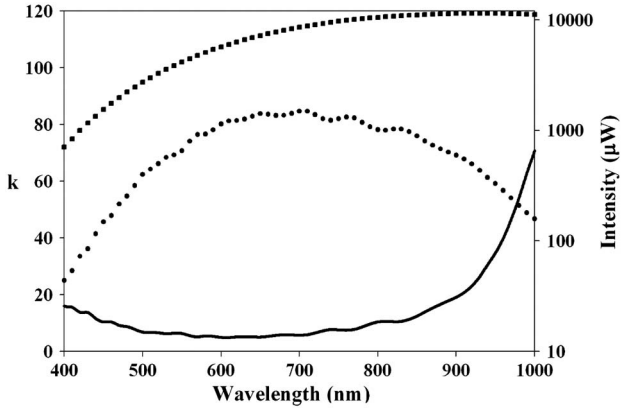

Fig. 14. The solid line is the k value curve of the calibrated irradiance of the ERL-HIS from 400 to 1000 nm. The left longitudinal coordinate is the coordinates of k curve. The right longitudinal coordinate has been taken as a logarithm and is the coordinate of the square dot and circle dot. The square dot is the response of the standard light source. The circle dot is the response of the ERL-HIS.

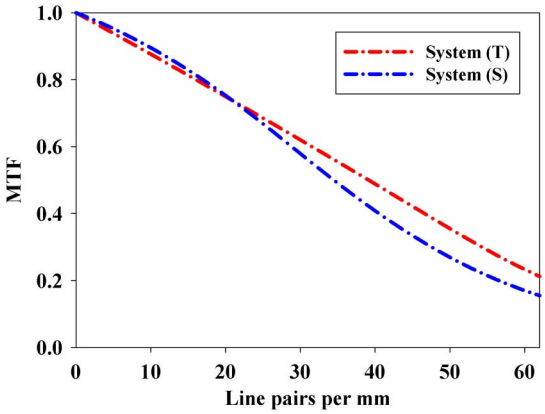

Fig. 15. (Color online) MTF of the ERL-HIS.

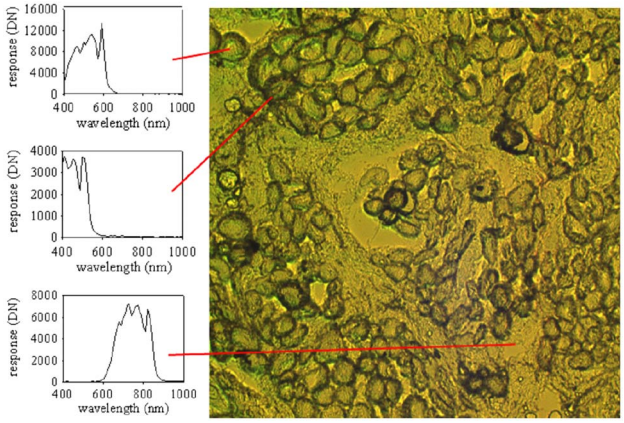

Fig. 17. (Color online) Picture of the oral cell, which is captured by the ERL-HIS.

different wavelengths and combined them to show on the control window of the software. Each pixel contained the spectrum showing the response from 400 to 1000 nm. Figure 17 plots the spectral information for the three pixels. The information was valuable and with the potential use of differentiating normal tissues from cancerous tissues.

4. Discussions and Conclusions

This paper presents a novel ERL-HIS that uses an embedded finite conjugate RL to perform a hyperspectral image without the need to move either the hyperspectrometer or the measured object. Simulation and analysis results indicate that the proposed system is feasible for practical applications, especially in observing and analyzing the biomedical image. The ERL-HIS has high resolution with spatial resolution of 30 μm × 8 μm and nominal spectral resolution of 2.8 nm. The tangential MTF is 30%, and the sagittal MTF is 20% at 62 lp/mm. This study implements the spectral calibration and radiometric calibration to ensure the accuracy of the hyperspectral data. This paper also designs a new (to our best knowledge) RL, which is a symmetric finite conjugate design consisting of 14 lenses with a total length of about 124 mm. The RL is a telecentric design; hence, the off-axis optical aberration is minimized. The simulations with ZEMAX confirm that within the entire wavelength range covered the optical performance of the ERL-HIS is stable in all fields, the distortion less than 0.01%, the field curvature less than 0.2 μm, the minimal rms radius 9.344 μm in the 4 mm field, and the lateral color smaller than 0.4 μm. Thus, the RL can project the image onto a scanning plane with excellent imaging quality and is suitable for HIS application.

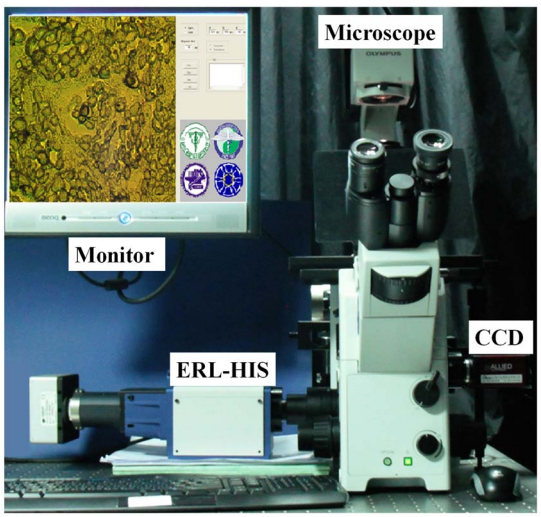

Fig. 16. (Color online) ERL-HIS attaches on the microscope.

The proposed ERL-HIS is superior to the traditional HIS in terms of design and fabrication of the RL module. First, a hyperspectral image depends on the scanning method to acquire data cube. The process could have opportunities for failure when the object, the hyperspectrometer, or both are moving. The proposed system spans the spatial domain onto a scanning plane through the embedded RL and facilitates image scanning inside the RL module such that the outside moving parts to move the object against the hyperspectrometer or vice versa can be completely removed from the mechanism. Second, owing to the change of the moving mechanism, the entire volume of the ERL-HIS is significantly reduced and the mechanism is simplified. The volume of the proposed ERL-HIS is about 50 cm (L)× 15 cm (W) × 13 cm (H). Although the proposed system adds the RL part, the volume is still smaller than the traditional system. Third, the proposed system is adaptive and compatible to various OMs. When the ERL-HIS attaches to various OMs, the optimization of the optical parameters, such as the alignment of the optical axis, can be easily done without the need of modifying the mechanism. For instance, Figure 16 shows the case of attaching the ERL-HIS to a microscope, in which the alignment of the optical axis and focus can be easily adjusted through the two screws outside the ERL-HIS box. Fourth, because of the design of the symmetric finite conjugate and telecentric RL, the off-axis optical aberration of the proposed system is minimized and optimized. The distortion is smaller than 0.01%, and the field curvature is smaller than 0.2 μm. Fifth, the

Table 1. Comparisons of ERL-HIS and Pushbroom System for Microscope Application

Mechanism	ERL-HIS + Microscope	Pushbroom + Microscope
Volume	75 cm (L) × 60 cm (W) × 80 cm (H)	120 cm (L) × 100 cm (W) × 90 cm (H)
Spectral range (nm)	400–1000	400–1000
$F/\#$	2.8	6.5
Spatial resolution	30 μm × 8 μm	20 μm × 9 μm
Spectral resolution (nm)	2.73	7.2
Throughput	>60%	>60%
Compatibility	Good	Bad
Scanning mechanism	SM	PZT
Off-axis aberration	Good	Bad
Cost	Low	High

previous scanning mechanism needs more stabilization and higher mechanical resolution to prevent scanning errors. However, the ERL-HIS uses the SM to replace the PZT because the RL utilizes the optical concept to change the scanning mechanism of the traditional HIS. The change reduces the mechanical resolution of scanning requirement but keeps the optical resolution. Additionally, the scanning time can be largely reduced, and the cost is much less compared to the traditional system. A comparison of the ERL-HIS and pushbroom hyperspectral system as used for microscope application is listed in Table 1. The pushbroom hyperspectral system combined with the microscope refers to Ref. [5] in this article.

In conclusion, this work has demonstrated the feasibility of the ERL-HIS by attaching it to a microscope for observing and diagnosing sliced cancer tissues sample *in vitro*. The proposed system is characterized by its higher scanning speed and optimized optical aberration. Other advantages include its lower cost, compactness, and compatibility with various OMs. We expect that the ERL-HIS can be applied to both basic and clinical biological research, such as differentiating cancer tissues from normal tissues. Efforts are under way in our laboratory to integrate fiber with the proposed system for biological and diagnostic applications in real-time fluorescent-spectral imaging. The proposed system can also be attached to a telescope for macroscopic-technical examination and documentation of artwork and for historical analysis.

This paper is particularly supported by the "Aim for the Top University Plan" of the National Chiao-Tung University and Ministry of Education, Taiwan, R.O.C., the National Science Council of Taiwan (NSCT) under contracts NSC 100-2220-E-009-033, NSC 99-2622-E-009-023-CC1, NSC 99-2218-E-039-001, and NSC 99-2631-H-034-001, and the Chung-Shan Institute of Science & Technology under contracts XV00E19P295 and CSIST-442-V302.

References

1. C. T. Willoughby, M. A. Folkman, and M. A. Figueroa, "Application of hyperspectral imaging spectrometer systems to industrial inspection," Proc. SPIE **2599**, 264–272 (1996).
2. C. Balas, V. Papadakis, N. Papadakis, A. Papadakis, E. Vazgiouraki, and G. Themelis, "A novel hyper-spectral imaging apparatus for the non-destructive analysis of objects of artistic and historic value," J. Cult. Herit. **4**, 330–337 (2003).
3. M. B. Sinclair, D. M. Haaland, J. A. Timlin, and H. D. T. Jones, "Hyperspectral confocal microscope," Appl. Opt. **45**, 6283–6291 (2006).
4. T. Pham, F. Bevilacqua, T. Spott, J. Dam, B. Tromberg, and S. Andersson-Engles, "Quantifying the absorption and reduced scattering coefficients of tissuelike turbid media over a broad spectral range with noncontact Fourier transform hyperspectral imaging," Appl. Opt. **39**, 6487–6497 (2000).
5. R. Schultz, T. Nielsen, J. Zavaleta, R. Ruch, R. Wyatt, and H. Garner, "Hyperspectral imaging: a novel approach for microscopic analysis," Cytometry **43**, 239–247 (2001).
6. M. E. Martin, M. B. Wabuyele, K. Chen, P. Kasili, M. Panjehpour, M. Phan, B. Overholt, G. Cunningham, D. Wilson, R. C. Denovo, and T. V. Dinh, "Development of an advanced hyperspectral imaging (HSI) system with applications for cancer detection," Ann. Biomed. Eng. **34**, 1061–1068 (2006).
7. Y. Garini, I. T. Young, and G. McNamara, "Spectral imaging: principles and applications," Cytom. A **69**, 735–747 (2006).
8. W. R. Johnson, D. W. Wilson, and G. Bearman, "All-reflective snapshot hyperspectral imager ultraviolet and infrared applications," Opt. Lett. **30**, 1464–1466 (2005).
9. Q. Li, Y. Xue, G. Xiao, and J. Zhang, "New microscopic pushbroom hyperspectral imaging system for application in diabetic retinopathy research," J. Biomed. Opt. **12**, 064011 (2007).
10. C. F. Cull, K. Choi, D. J. Brady, and T. Oliver, "Identification of fluorescent beads using a coded aperture snapshot spectral imager," Appl. Opt. **49**, B59–B70 (2010).
11. B. Ford, M. Descuor, and R. Lynch, "Large-image-format computed tomography imaging spectrometer for fluorescence microscopy," Opt. Express **9**, 444–453 (2001).
12. L. Gao, R. T. Kester, N. Hagen, and T. S. Tkaczyk, "Snapshot image mapping spectrometer (IMS) with high sampling density for hyperspectral microscopy," Opt. Express **18**, 14330–14344 (2010).
13. R. T. Kester, L. Gao, and T. S. Tkacyzk, "Development of image mappers for hyperspectral biomedical imaging application," Appl. Opt. **49**, 1886–1899 (2010).
14. W. J. Smith, *Modern Optical Engineering* (McGraw-Hill, 2000).
15. D. Malacara, *Geometrical and Instrumental Optics* (Academic, 1988).
16. R. E. Fisher and B. T. Galeb, "Performance evaluation and optical testing," in *Optical System Design* (SPIE, 2000), pp. 301–313.